Journal of Sol-Gel Science and Technology (2021) 99:527–533
https://doi.org/10.1007/s10971-021-05589-9

ORIGINAL PAPER: NANO-STRUCTURED MATERIALS (PARTICLES, FIBERS, COLLOIDS, COMPOSITES, ETC.)

Synthesis of $CoFe_2O_4$ superparamagnetic nanoparticles using a rapid thermal processing furnace with halogen lamps

André de Oliveira Girão Maia[1,2] · Francisco Gilvane Sampaio Oliveira[1] · Carlos Henrique Nascimento Cordeiro[3] · Edwalder Silva Teixeira[1] · Erandir Brasil da Silva · João Maria Soares[3,4] · Igor Frota de Vasconcelos[1,5] · José Marcos Sasaki[1,6] · Thomas Dumelow[3,4]

Received: 10 March 2021 / Accepted: 4 July 2021 / Published online: 11 August 2021
© The Author(s), under exclusive licence to Springer Science+Business Media, LLC, part of Springer Nature 2021

Abstract

This work deals with the synthesis of superparamagnetic cobalt ferrite ($CoFe_2O_4$) nanoparticles, via a sol-gel method that uses gelatin as an organic precursor and a rapid thermal processing furnace with halogen lamps as a heat source. TEM, HRTEM, XRD, VSM and Mössbauer spectroscopy measurements were performed, at room temperature, to characterize the samples. Nanoparticles with an average size of 5–10 nm and microstrain of the order of 10^{-4}–10^{-3} were obtained. Magnetic hardening was also observed with increased nanoparticle size, in addition to an increase in the anisotropy constant, which ranged from 1.7 to $4.7{\cdot}10^6$ erg/cm^3. The saturation magnetization decreased with decreasing size due to the formation of a magnetically dead layer on the surface (thickness = 0.6–0.7 nm). The Mössbauer spectra showed an increase in the superparamagnetic phase for samples with smaller nanoparticles and less dispersion.

Graphical Abstract

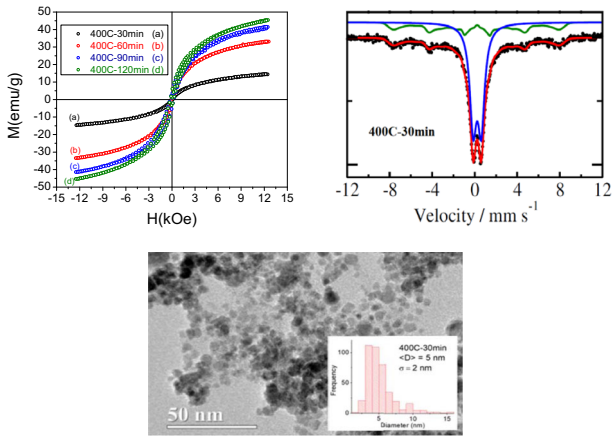

✉ André de Oliveira Girão Maia
giraomaia@gmail.com

[1] Programa de Pós-Graduação em Engenharia e Ciência de Materiais, Centro de Tecnologia, Universidade Federal do Ceará, Campus do Pici - Bloco 729, Fortaleza, CE 60.440-554, Brazil

[2] Instituto Federal de Educação, Ciência e Tecnologia do Rio Grande do Norte, Campus Mossoró, Rua Raimundo Firmino de Oliveira 400, Conj. Ulrick Graaf, Mossoró, RN 59.628-330, Brazil

[3] Programa de Pós-Graduação em Física, FANAT, Universidade do Estado do Rio Grande do Norte, Campus Universitário Central, Setor II, Mossoró, RN 59.610-090, Brazil

[4] Departamento de Física, FANAT, Universidade do Estado do Rio Grande do Norte, Campus Universitário Central, Setor II, Mossoró, RN 59.610-090, Brazil

[5] Departamento de Engenharia Metalúrgica e de Materiais, Centro de Tecnologia, Universidade Federal do Ceará, Campus do Pici - Bloco 729, Fortaleza, CE 60.440-554, Brazil

[6] Departamento de Física, Centro de Ciências, Universidade Federal do Ceará, Campus do Pici - Bloco 922, Fortaleza, CE 60.440-900, Brazil

Keywords Nanoparticles · Cobalt ferrite · Superparamagnetic · Sol–gel preparation · Halogen lamps furnace

Highlights

- The protein sol–gel method using gelatin is a fast and low-cost process for the production of nanoparticulate powders.
- The use of RTP furnaces in calcination helps to control the energy supplied to the sample.
- The advantages of using halogen lamps in RTP furnaces are low cost, uniform heating, and good temperature control.
- In order to have a superparamagnetic material, it is necessary to produce nanoparticles with a size below a critical size.

Abbreviations

RTP	rapid thermal processing
RTP-HL	halogen lamp RTP systems
Sch	Scherrer's formula
WHP	Williamson–Hall plot
SSP	size–strain plot
XRD	X-ray diffraction
TEM	transmission electron microscopy
HRTEM	high-resolution transmission electron microscopy
VSM	vibrating-sample magnetometry

1 Introduction

The production and control of the size and morphology of nanoparticles are some of the most researched subjects in the scientific community [1–4]. Producing nanoparticles with an increasingly smaller size with a specific shape, using the least amount of energy, are the main objectives [5–7]. Reducing the size of the nanoparticles may allow the appearance of a new magnetic property or reinforce an existing property [4, 8]. One of the ways to achieve this is by controlling the heat supply during synthesis, as heat favors the growth of nanoparticles [5–8]. The use of RTP (rapid thermal processing) systems is highly recommended in these cases as they have high heating rates, thus reducing the calcination time, in addition to having high cooling rates [5, 6, 8–12]. Halogen lamp RTP systems (RTP-HL) can achieve a heating rate of up to hundreds of K/s, while conventional systems can only reach a few tens of K/min [5]. The advantages of using halogen lamps are: low cost, uniform heating, and good temperature control [5]. RTP systems are also used to control the crystallization of amorphous phases, control phase transitions, reduce strains in the crystalline structure, produce crystallographic texture [5], change coercivity [8, 9, 11], and increase magnetic permeability [12].

Zeng et al. [9] used the RTP technique with halogen lamps, whose heating rate was 200 °C/min, to show that FePt nanoparticles produced in the RTP furnace had greater coercivity than those produced in a conventional furnace. Corbiere et al. [7] produced vanadium nitride nanoparticles using a halogen lamp furnace and whose heating rate was 50 K/min, obtaining nanoparticles smaller than 10 nm. Chu et al. [6] produced nanocomposites with NdFeB and realized that the samples produced in an RTP system, when compared to samples produced in a conventional furnace, showed a reduction in grain size, greater morphological uniformity in addition to an increase in coercivity.

It is known that cobalt ferrite has cubic magnetocrystalline anisotropy, several axes of easy magnetization, reasonable saturation magnetization, positive anisotropy constant, and good mechanical and chemical stability. Due to these characteristics, it is well suited for the production of permanent and isotropic magnets, magnetic recording, magnetic fluids, guided drug delivery, medical diagnoses, hyperthermia treatment, etc. For this to be possible it is necessary to produce stable particles with a single magnetic domain. It is estimated that to occur the formation of a single domain it is necessary that the particles have a size between 7–10 nm. In form bulk, cobalt ferrite is a hard magnetic material with a Curie temperature around 790 K [1, 3, 4]. Grigorova et al. [1] showed in his work that cobalt ferrite nanoparticles have saturation magnetization ranging from 13–70 emu/g, remanence ranging from 1–23 emu/g, and coercivity ranging from 0.07 to 1.75 kOe. Kumar et al. [3] showed in their work that the saturation magnetization ranged from 2 to 50 emu/g, the remanence ranged from 0.5 to 25 emu/g and coercivity ranged from 0.5 to 1.4 kOe. Rajendran et al. [4] showed in his work that the saturation magnetization ranged from 9 to 49 emu/g, the remanence ranged from 0.55 to 7 emu/g and zero coercivity.

2 Experimental

The samples were prepared by the protein sol-gel method that uses gelatin as an organic precursor [13]. Initially 4.000 g of gelatin was dissolved in 10 mL of distilled water at room temperature. Then 8.000 g of $Fe(NO_3)_3{\cdot}9H_2O$ was also dissolved in 10 mL of distilled water, at room temperature. The two solutions were then mixed in beaker I. The same sequence was performed with 2.8820 g of $Co(NO_3)_2{\cdot}6H_2O$ and 1.4419 g of gelatin and placed in a beaker II. The solutions of beakers I and II were then mixed and subjected to magnetic stirring for 1 h at room temperature.

The final solution was put to dry in a furnace at 100 °C for 48 h. The xerogel formed was macerated and calcined at 400 °C for 30, 60, 90, and 120 min in the RTP furnace with halogen lamps (heating rate: 100 °C/min). Due to a cooling system, the furnace returned to room temperature in ~1 h. The sample calcined was washed with hydrogen peroxide to eliminate the remaining organic matter. Then it was centrifuged and dried in a furnace at 100 °C for 48 h. Finally, X-ray diffraction (XRD), transmission electron microscopy (TEM), high-resolution transmission electron microscopy (HRTEM), vibrating-sample magnetometry (VSM), and Mössbauer spectroscopy measurements were made.

Cobalt ferrite (bulk) has a cubic unit cell, with space group Fd-3m (227) and cell parameters $a = b = c =$ 0.83919 nm (ICDD 00-022-1086). Its structure can be inverse spinel or mixed spinel, the latter occurring more frequently [3, 14, 15].

The XRD measurements were performed at room temperature in a PanAlytical diffractometer, model X'Pert Pro (MPD), operated at 40 kV and 40 mA, with a cobalt target ($\lambda_{K\alpha 1} = 0.1789$nm) and hybrid monochromator. The diffraction patterns were obtained in the range 2θ: 10°–100° with 0.013° step and a speed of 100 s per step. The crystalline phases were identified using the X'Pert HighScore Plus 3.0d software. TEM and HRTEM measurements were performed at room temperature in a transmission electron microscope model Jeol (JEM-2100), equipped with EDS, Thermo Scientific. The VSM measurements were performed at room temperature using a vibrating sample magnetometer whose magnetic field ranged from −12 kOe to +12 kOe. The Mössbauer spectra were measured at room temperature in a SEECo Spectrometer, Model W302, with a radioactive source diffused in a rhodium matrix and were adjusted with NORMOS software, using the hyperfine field distribution method.

3 Results and discussion

From the XRD measurements (Fig. 1a), it is observed that the cubic cobalt ferrite phase was formed in all samples. The average size D of the nanoparticles was determined by Scherrer's Formula (Sch) $D = k\lambda/(\beta\cos\theta)$ [16], by a linear fit of the Williamson–Hall Plot (WHP) $\beta\mathrm{Cos}\theta/\lambda = k/D + 4\varepsilon\sin\theta/\lambda$ [17] and by the linear fit of the Size–Strain Plot (SSP) $(d\beta\cos\theta/\lambda)^2 = (k/D)^2 d^2 + 2\pi\langle\varepsilon\rangle^2$ [18]. The microstrain ε and its root mean squar value, $\langle\varepsilon\rangle$, were calculated from linear fits to the WHP and SSP, respectively. As the nanoparticles were approximately spherical in shape, the value chosen for the form factor was $k = 1$ [16]. The value of d (d-spacing) is calculated by Bragg's Law. It can be seen from Table 1 that the size of the nanoparticles increased with increasing calcination time. This is because the growth of nanoparticles and coalescence are stimulated by the supply of energy. It is also observed that the microstrain oscillated, despite the fact that it was expected to decrease with the increase of the calcination time, since the crystalline structure approaches the ideal with the energy supply [19].

Single-domain particles exhibit superparamagnetic behavior below a certain critical size D_C [15, 19]. For a system of spherical, single-domain and uniaxial nanoparticles, of $CoFe_2O_4$, with low size dispersion, the value of D_C is in the range 8–10 nm [4, 15, 20]. In Fig. 1b and c we have the TEM and HRTEM images of samples 400C-30 min and 400C-120 min, respectively, where it is possible to observe the approximately spherical shape of the nanoparticles, with the sample 400C-30 min having a smaller average and less dispersion (smaller standard deviation σ). Through HRTEM images it was possible to visualize crystalline planes and to identify them from the d-spacing: 0.29 nm (220) and 0.48 nm (111). Figure 2a and Table 1 show that saturation magnetization (M_S), maximum field magnetization (M_{max}), remanant magnetization (M_R) and coercivity (H_C) increased with the increase in the size of the nanoparticles and this increased the number of blocked particles. Consequently, we have a gain in the ferrimagnetic phase for samples with a larger nanoparticle size. By making a fit to the magnetization curve, by the saturation approximation law $M = M_s[1-0.0762K^2/(M_s^2 H)]$ [21], it was possible to determine the values of M_s and K (anisotropy constant) for each sample. The anisotropy constant, which represents an energy density, increased with increasing average size, since larger nanoparticles have more atoms and thus store more energy due to magnetization. The K value fell in the range $1.7–4.7 \cdot 10^6$ erg/cm^3, which is in line with the results found by Machado et al. [19], Babić-Stojić et al. [22], and Mooney et al. [15]. According to Vázquez-Vázquez et al. [21], magnetic nanoparticles do not have uniform magnetization, but their magnetization decreases from the center to the surface, and on the surface there is a layer, of thickness t, with zero magnetization, called the dead layer. It is possible to determine the value of this thickness t using the dead layer model $M_s = \mathrm{Ms}(bulk)[1–6t/\langle D\rangle]$ [21], where Ms (bulk) is the saturation magnetization of a bulk sample and $\langle D\rangle$ is the average size measured by TEM images. Figure 2b shows that $t = 0.6$ nm and $M_s(\mathrm{bulk}) = 89.11$ emu/g, which is in accordance with the results obtained by the TEM measurements in Fig. 1, and those obtained by Vázquez-Vázquez et al. [21] and by Mooney et al. [15]. For samples with the lowest average size values, this layer is responsible for significant reductions in saturation magnetization and maximum field magnetization (see Fig. 2 and Table 1).

Figure 3 shows the ZFC (zero-field cooled) and FC (field cooled) curves of the 400C-30 min sample measured

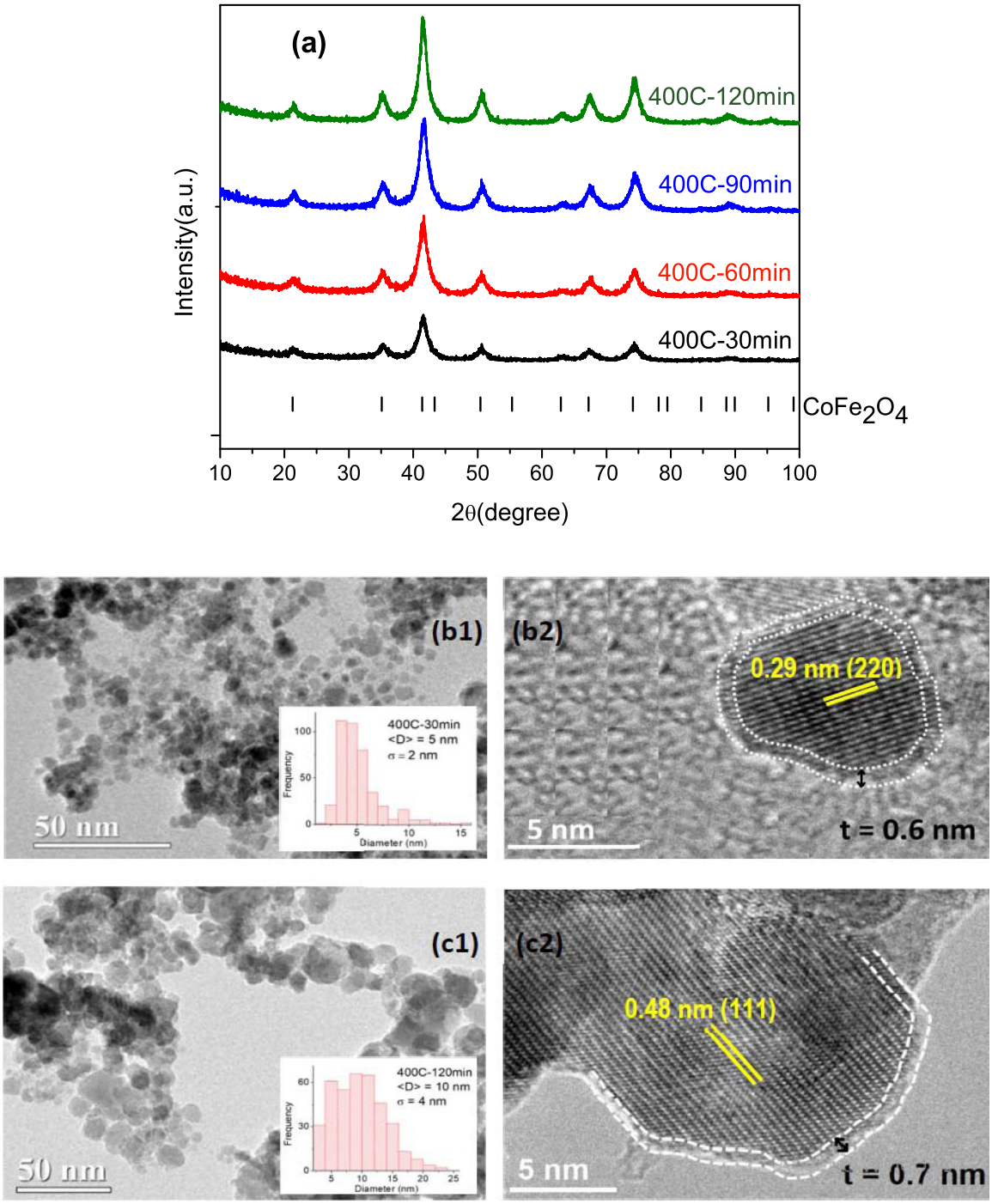

Fig. 1 **a** XRD of the four samples (ICDD 00-022-1086). **b** and **c** TEM, HRTEM and histograms of samples 400C-30 min and 400C-120 min, respectively

Table 1 Average size, microstrain and magnetic measurements

400 °C	Average size (nm)				Microstrain		Magnetic measurements				
							emu/g			kOe	-10^6 erg/cm^3
	TEM	Sch	WHP	SSP	WHP	SSP	M_S	M_{max}	M_R	H_C	K
30 min	5	6	7	7	$2{\cdot}10^{-3}$	$3{\cdot}10^{-3}$	18	15	0.04	0.04	1.7
60 min	6	6	6	6	$3{\cdot}10^{-4}$	$2{\cdot}10^{-3}$	39	33	1.20	0.06	2.9

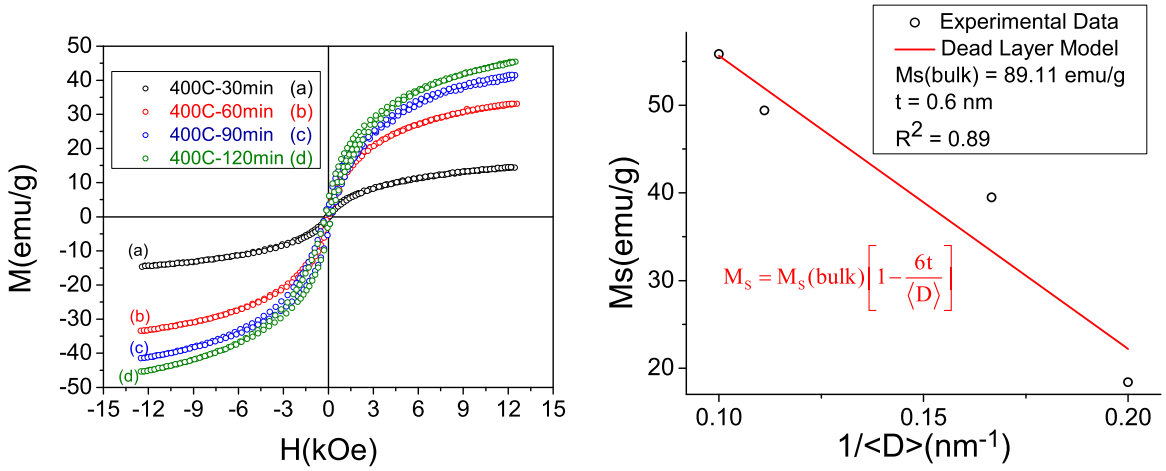

Fig. 2 **a** *M* versus *H* measurements of the four samples and **b** Linear Fit of the Dead Layer Model

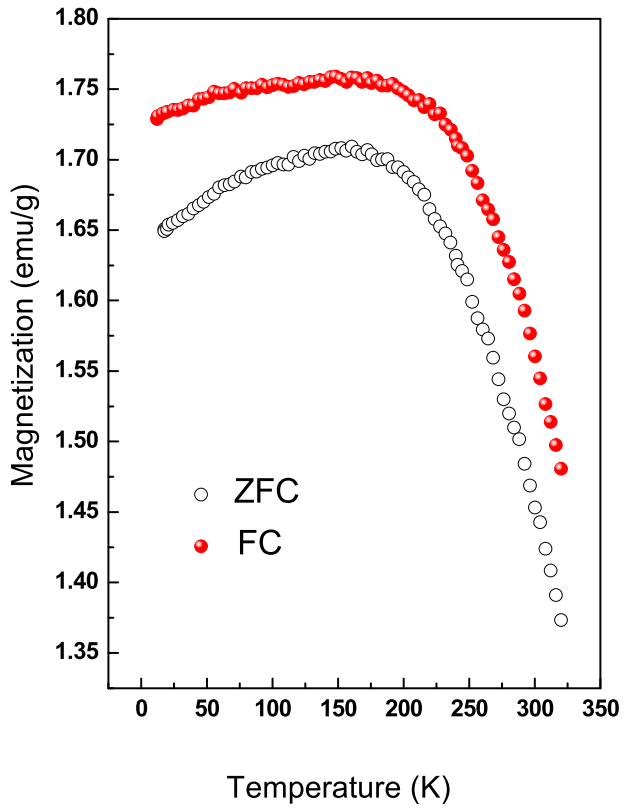

Fig. 3 ZFC–FC curves of sample 400C-30 min under 100 Oe magnetic field

in the temperature range between 10 and 330 K under the application of a 100 Oe magnetic field. As the temperature increases, the magnetization referring to the ZFC curve also increases until reaching a maximum magnetization value of 1.71 emu/g around 165 K (blocking temperature). However, even after the transition from the blocked to the superparamagnetic state, the ZFC–FC curves do not overlap to reach a temperature of magnetic irreversibility. Therefore, these results indicate that we have, at room temperature, a system composed of strongly interacting superparamagnetic nanoparticles.

Figure 4 shows the Mössbauer spectra, measured at room temperature, for all samples. The 400C-120 min sample showed a distribution of hyperfine fields (B_{fh}) centered at 48T, characteristic of the α-magnetite phase [23]. However, it is possible to observe in the spectra of samples 400C-90 min, 400C-60 min, and 400C-30 min a doublet with quadrupole splitting values of 0.77, 0.76, and 0.90 mm/s, characteristic of the superparamagnetic phase, induced by the effect of reducing the size of the nanoparticles [23]. In addition, the ferrimagnetic contributions of the samples are not completely suppressed, since, in all spectra, a distribution of B_{fh} is identified, showing the superposition of the ferrimagnetic and superparamagnetic phases. The analysis of the spectral area relationship between the doublet and the sextet shows that the superparamagnetic phase present in samples 400C-90 min, 400C-60 min, and 400C-30 min corresponds to 15%, 44%, and 68%, respectively. Such behavior is a reflection of the reduction in size, which induces the superparamagnetic phase. Such results are in agreement with the TEM, XRD, and VSM analyses.

4 Conclusion

It was concluded that the sol–gel process, together with the RTP-HL furnace, was efficient in producing superparamagnetic nanoparticles of cobalt ferrite. It was observed that the increase in the calcination time increased the size of the nanoparticles and caused magnetic hardening, but the microstrain underwent unexpected changes. The increase in size of the nanoparticles also caused an increase in the saturation magnetization

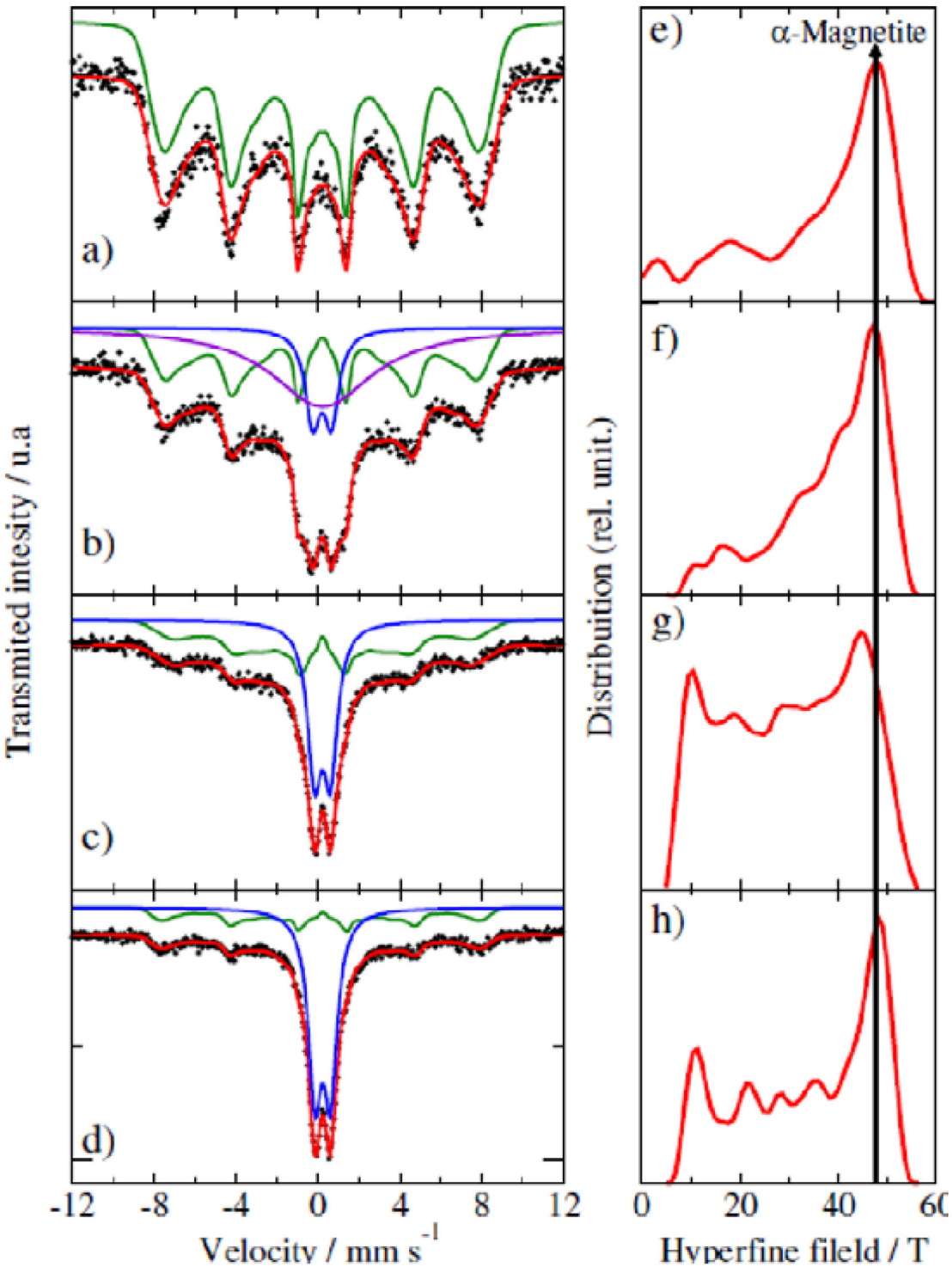

Fig. 4 Mössbauer spectra of the samples and distribution of hyperfine fields. **a–e** 400C-120 min, **b–f** 400C-90 min, **c–g** 400C-60 min, and **d–h** 400C-30 min

and in the anisotropy constant. The thickness of the dead layer that covered the nanoparticles was estimated to be 0.6 nm. Magnetization measurements indicated a blocking temperature close to 165 K. The results of the Mössbauer spectra showed that the samples with the smaller average size (5–6 nm) have a higher fraction of the super-paramagnetic phase and, consequently, lower coercivity values.

Acknowledgements We are grateful to the Laboratório de Materiais Avançados at the Universidade Federal do Ceará, to the Laboratório de Medidas Ópticas e Magnéticas at the Universidade do Estado do Rio Grande do Norte, and to the Laboratório Multiusuário de Microscopia de Alta Resolução at the Universidade Federal de Goiás. We also thank CNPq and CAPES for their financial support.

Conflict of Interest There are no conflicts of interest. The research that originated this article had financial support from CAPES (Coordination for the Improvement of Higher Education Personnel) and CNPq (National Council for Scientific and Technological Development) and has already been commented on and given the due gratitude they demand. The partner laboratories LAMOP (Laboratório de Medidas Ópticas e Magnéticas - UERN), LABMIC (Laboratório Multiusuário de Microscopia de Alta Resolução - UFG) and the Advanced Materials Laboratory - UFC also require only acknowledgments at the end of the article.

Publisher's note Springer Nature remains neutral with regard to jurisdictional claims in published maps and institutional affiliations.

References

1. Grigorova M, Blythe HJ, Blaskov V, Rusanov V, Petkov V, Masheva V, Nihtianova D, Martinez LlM, Muñoz JS, Mikhov M (1998) Magnetic properties and Mössbauer spectra of nanosized $CoFe_2O_4$ powders. J Magn Magn Mater 183:163–172. https://doi.org/10.1016/S0304-8853(97)01031-7
2. Carpenter EE (2001) Iron nanoparticles as potential magnetic carriers. J Magn Magn Mater 225:17–20. https://doi.org/10.1016/S0304-8853(00)01222-1
3. Kumar L, Kar M (2011) Effect of annealing temperature and preparation condition on magnetic anisotropy in nanocrystalline cobalt ferrite. IEEE Trans Magn 47:3645–3648. https://doi.org/10.1109/TMAG.2011.2151841
4. Rajendran M, Pullar RC, Bhattacharya AK, Das D, Chintalapudi SN, Majumdar CK (2001) Magnetic properties of nanocrystalline $CoFe_2O_4$ powders prepared at room temperature: variation with crystallite size. J Magn Magn Mater 232:71–83. https://doi.org/10.1016/S0304-8853(01)00151-2
5. Jin ZQ, Liu JP (2006) Rapid thermal processing of magnetic materials. J Phys D: Appl Phys 39:R227–R244. https://doi.org/10.1088/0022-3727/39/14/R01
6. Chu K-T, Jin ZQ, Chakka VM, Liu JP (2005) Rapid magnetic hardening by rapid thermal annealing in NdFeB-based nanocomposites. J Phys D: Appl Phys 38:4009–4014. https://doi.org/10.1088/0022-3727/38/22/002
7. Corbiere TCM, Ressnig D, Giordano C, Antonietti M (2013) Focused radiation heating for controlled high temperature chemistry, exemplified with the preparation of vanadium nitride nanoparticles. RSC Adv 3:15337–15343. https://doi.org/10.1039/C3RA41040D
8. Yano K, Nandwana V, Poudyal N, Rong C-B, Liu JP (2008) Rapid thermal annealing of FePt nanoparticles. J Appl Phys 104:013918. https://doi.org/10.1063/1.2953078
9. Zeng H, Sun S, Sandstrom RL, Murray CB (2003) Chemical ordering of FePt nanoparticle self-assemblies by rapid thermal annealing. J Magn Magn Mater 266:227–232. https://doi.org/10.1016/S0304-8853(03)00482-7
10. Koteeswara Reddy N, Ahsanulhaq Q, Hahn YB (2009) Influence of RTA treatment on the physical properties of well-aligned ZnO nanorods. Physica E 41:368–372. https://doi.org/10.1016/j.physe.2008.08.061
11. Roozeboom F, Dirne FWA (1995) Rapid thermal annealing of amorphous and nanocrystalline soft-magnetic alloys in a static magnetic field. J Appl Phys 77:5293–5297. https://doi.org/10.1063/1.359283
12. Roozeboom F, Abedrabbo S, Ravindra NM, Walk H, Falter M (1998) Rapid thermal magnetic annealing as an emerging technology in field-annealing of thin magnetic films for recording heads. Mater Sci Semiconductor Proces 1:303–315. https://doi.org/10.1016/S1369-8001(98)00024-9
13. Maia AOG, Meneses CT, Menezes AS, Flores WH, Melo DMA, Sasaki JM (2006) Synthesis and X-ray structural characterization of NiO nanoparticles. J Non-Cryst Solids 352:3730–3733. https://doi.org/10.1016/j.jnoncrysol.2006.03.103
14. Kumar L, Kar M (2011) Influence of Al^{3+} ion concentration on the crystal structure and magnetic anisotropy of nanocrystalline spinel cobalt ferrite. J Magn Magn Mater 323:2042–2048. https://doi.org/10.1016/j.jmmm.2011.03.010
15. Mooney KE, Nelson JA, Wagner MJ (2004) Superparamagnetic cobalt ferrite nanocrystals synthesized by alkalide reduction. Chem Mater 16:3155–3161. https://doi.org/10.1021/cm040012
16. Scherrer P, Bestimmung der Grösse und der inneren Struktur von Kolloidteilchen mittels Röntgenstrahlen, Mathematisch-Physikalische Klasse (1918) 98–100, https://eudml.org/doc/59018 (Accessed 23 Nov 2020).
17. Williamson GK, Hall WH (1953) X-ray line broadening from filed aluminium and wolfram. Acta Metallurgica 1:22-31, http://www.xray.cz/xray/csca/kol2011/kurs/dalsi-cteni/clanky/Williamson-ActaMet-1953-1-22-WH-Plot.pdf (Accessed 23 Nov 2020).
18. Manniamal K, Madhu G, Biju V (2017) X-ray diffraction line profile analysis of nanoestructured nickel oxide: shape factor and convolution of crystallite size and microstrain contributions. Physica E 85:214–222. https://doi.org/10.1016/j.physe.2016.08.035
19. Machado FLA, Soares JM, Conceição OLA, Choi ES, Balicas L (2017) Magnetic properties of the nanocomposite $CoFe_2O_4$/FeCoFeO at a high H/T regime. J Magn Magn Mater 424:323–326. https://doi.org/10.1016/j.jmmm.2016.10.079
20. Liu C, Zou B, Rondinone AJ, Zhang ZJ (2000) Chemical control of superparamagnetic properties of magnesium and cobalt spinel ferrite nanoparticles through atomic level magnetic couplings. J Am Chem Soc 122:6263–6267. https://doi.org/10.1021/ja000784g
21. Vázquez-Vázquez C, López-Quintela MA, Buján-Núñez MC, Rivas J (2011) Finite size and surface effects on the magnetic properties of cobalt ferrite nanoparticles. J Nanopart Res 13:1663–1676. https://doi.org/10.1007/s11051-010-9920-7
22. Babić-Stojić B, Jokanović V, Milivojević D, Jagličić Z, Makovec D, Jović N, Marinović-Cincović M (2013) Magnetic and structural studies of $CoFe_2O_4$ nanoparticles suspended in an organic liquid. J Nanomater 2013, https://doi.org/10.1155/2013/741036.
23. Dyar MD, Agresti DG, Schaefer MW, Grant CA, Sklute EC (2006) Mössbauer spectroscopy of earth and planetary materials. Annu Rev Earth Planet Sci 34:83–125. https://doi.org/10.1146/annurev.earth.34.031405.125049